ISSN 1512-1461

UDC: 538.9 Condensed matter Physics, Solid state Physics, Theoretical Condensed matter Physics

ENHANCING THE PHOTOCURRENT OF SPIN COATED CuO THIN FILMS USING TX 100 SURFACTANT

P. Samarasekara [1], P. G. D. C. K. Karunarathna [2], B. M. C. M. Bandaranayake [1] and C. A. N. Fernando [2]

[1]Department of Physics, University of Peradeniya, Peradeniya, Sri Lanka
[2]Department of Nano Science Technology, Wayamba University of Sri Lanka, Kuliyapitiya, Sri Lanka

Abstract:
CuO films were synthesized at spin speed of 2000 rpm for 30 s by spin coating, and subsequently annealed at 500 ^{0}C for an hour in air. Structural, optical, chemical and electrical properties of spin coated CuO films with and without the TX 100 surfactant were compared. The XRD patterns, UV-Visible absorption spectrums and I-V characteristics curves were employed to study the structural, optical and electrical properties of the CuO samples. The chemical properties of the CuO thin films were determined by the FTIR spectrums. Single phase of CuO could be crystallized under these annealing conditions. FTIR spectrums also confirm the formation of CuO bonds. Photovoltaic properties were determined using a liquid junction photocell prepared with KI electrolyte. Photocurrent could be remarkably enhanced by adding the TX-100 surfactant to initial copper acetate solution. The addition of the TX 100 surfactant increased the photocurrent, photovoltage and the output power by factors of 2.12, 1.71 and 4.26, respectively. According to the XRD patterns, the crystallite size increased after adding the TX 100 surfactant. According to the UV-Visible spectrums, the optical band gap increases due to the TX 100 surfactant. According to the impedance data, the samples indicate the electrochemical cell behavior. Two semicircles can be observed in Nyquist plots. Life times of the electrons in the CuO thin films were calculated using Bode phase diagrams.

Keywords: *Cupric Oxide, spin coating, UV-visible spectrums, TX-100 surfactant, photovoltaic properties*

1. Introduction:

Cupric oxide (CuO) is vastly used in solar cells, gas sensors, nanoelectronics, spintronics, superconductors, electrochemical cells and diodes. CuO is a black color material with band gap in the range of 1.2 to 1.9eV. However, the band gap CuO thin films is slightly higher than that of bulk CuO. CuO nanostructured films have been synthesized by free oxidation of sputtered Cu_2O nanoporous films in alkaline solution. The optical band gap of these nanostructured CuO films was found to be 2.15 eV [1]. In addition, CuO layers were applied to enhance ultraviolet photodetectors established on In_2O_3 nanowires. These light sensors fabricated on hybrid materials have indicated high quality crystalline nature with low response time and broader spectral range in addition to high photoconductive gain [2]. Cr doped CuO films fabricated by DC pulsed magnetron sputtering at 100 ^{0}C have been characterized. Sensor response and selectivity towards acetone in dry air have been improved by doping Cr to CuO films [3]. Zn^{2+} doped CuO films have been synthesized by spin coating. Highest output power of liquid junction photocell with KI electrolyte has been obtained for film with doping concentrations of 6%. Highest photovoltage has been reported for the doping concentration of 10% [4]. CuO films have been

ISSN 1512-1461

synthesized by successive ionic layer adsorption and reaction method for different pH values. Increasing pH value has decreased the band gap. In addition, the refractive index has decreased with the decrease of pH value [5].

CuO thin films have been grown by chemical solution method with layer variation. Band gap of these CuO films has decreased from 2.05 to 1.89 eV as the annealing temperature was increased [6]. CuO films have been deposited by direct current reactive magnetron sputtering which was found to be a reproducible technique. CuO/CdS p-n junction solar cell prepared with these CuO films have provided an open circuit photovoltage of 421 mV, short circuit current density of 3.6 mA/cm^2, fill factor of 0.46 and efficiency of 1.2% [7]. CuO thin films have been fabricated on glass substrates by sol-gel spin coating technique. Films annealed at 550 ^0C have indicated the highest absorbance [8]. Multilayers of CuO and ZnO have been synthesized by spin coating and subsequently annealed at 500 ^0C in air for one hour to crystallize the oxide phase. The multilayer with ZnO as the top layer has provided a higher output power of 3.6 $\mu W/cm^2$ compared to the output power of a multilayer with CuO as the top layer (1.1 $\mu W/cm^2$) [9]. CuO and Cu_2O thin films have been deposited on Si(111), glass and quartz substrates by magnetron sputtering. The influence of the nature of the substrates on formation of Cu_2O and CuO phases has been investigated [10]. Copper oxide thin films have been fabricated on normal glass substrates by sputtering at $5x10^{-5}$ mbars. The effect of deposition power on electrical and optical properties has been investigated [11]. The variation of particle size, strain and dislocation density of Zn^{2+} doped CuO films with doping concentration has been studied. The particle size, dislocation density, strain and optical band gap have a turning point close to the doping concentration of 6% [12].

Thin films of CuO have been grown on glass substrates at different substrate temperatures by chemical spray pyrolysis technique. The mobility and the carrier concentration have been improved by annealing samples [13]. Modified successive ionic layer adsorption and reaction method has been employed to synthesize CuO on glass substrates. Properties of films have been investigated for different numbers of deposition cycles and different reaction times [14]. Low dimensional nanocomposite bilayer CuO/ZnO solar cells have been deposited by vapor deposition techniques at different various annealing temperatures. Power conversion efficiency has been improved by increasing the annealing temperature [15]. CuO and CuO/graphene nanostructured thin films have been fabricated by a doctor blade coating method for counter electrodes in Pt-free dye sensitized solar cells [16]. CuO is a favorable replacement for expensive Pt electrodes, because oxide layers can be synthesized by inexpensive techniques. Cu_2O and CuO layers have been grown on the surface of a copper foil by chemical and anodic oxidation. The composition of initial forming layer depends on the current density used in the anodic oxidation [17]. Ordered mesoporous ZnO nanoparticles have been fabricated by a template method. CuO layer has been deposited on the ZnO layer. In_2O_3 has been added to this ZnO/CuO layer to construct a room temperature gas sensor [18]. Physical properties of nanostructured CuO films have been improved by adding TX-100 surfactant. CuO films with preferred orientations have been synthesized using the TX-100 surfactant [19]. Nanocrystals of Cu_2O and CuO have been fabricated by a hot-soap method to detect H_2S gas. Cu_2O thin films fabricated by spin coating method have been able to detect H_2S concentrations from 1 to 8 ppm at 50-150 ^0C [20].
Because spin coating method is faster and lower in cost, the spin coating technique is applied to deposit many materials for different applications. Zn doped hydroxyapatite films have been synthesized by sol-gel spin coating. Biocompatibility assays indicated that these films did not indicate any toxicity towards the HeLa cells [21]. Cloisite-15A dispersed polyvinylidene fluoride nanocomposite thin films have been grown by spin coating technique for sensor applications [22]. ZnO thin films have been synthesized by spin coating to detect NO_2, NH_3, CH_3OH, Cl_2 and H_2S gases [23]. ZnO thin films with nanorod morphology have been deposited using a two step process consisting of sol-gel spin coating

ISSN 1512-1461

and solvothermal methods [24]. SnO_2 thin films have been fabricated by spin coating on glass substrates [25]. Carbon nanotubes were fabricated using a chemical vapor deposition by us [26]. Previously thin films have been synthesized using expensive techniques incorporated with vacuum by us [27, 28]. CuO indicates room temperature ferromagnetism. The magnetic properties have been investigated using modified Heisenberg Hamiltonian by us [29-35].

Structural, optical, chemical and electrical properties of spin coated CuO films prepared with and without the TX 100 surfactant are presented in this manuscript. Structural properties were investigated using X-ray diffraction (XRD) patterns. Chemical properties were determined by Fourier Transform Infra-red (FTIR) spectrometry. UV-Visible spectrometer was employed to study the optical properties. Photocurrent could be improved by adding the TX 100 surfactant to the initial solution of copper acetate and isopropyl alcohol. TX 100 surfactant was replaced by diethanolamine in the samples prepared without the TX 100 surfactant. The data of the CuO thin film samples prepared with diethanolamine have been presented in some of our previous publications [4, 9, 12]. However, the structural properties of the CuO samples did not change due to the addition of the TX 100 surfactant.

2. Experimental:

Copper acetate was measured and put in to a properly clean small container and required amount of isopropyl alcohol was added to it. Thereafter, one drop of the TX 100 surfactant ($C_{14}H_{22}O(C_2H_4O)_n$) was added to the solution. The solution was stirred for about 24 hour by using a magnetic stirrer at room temperature. Then thin layer of above solution was deposited on top of the properly cleaned glass plate or conducting glass plate using a spin coater (2000 rpm) for 30s. Finally the spin coated sample was annealed at 500 ^{0}c for an hour in a box furnace. Samples were prepared with and without the TX 100 surfactant. Diethanolamine was added to copper acetate and isopropyl alcohol solution to synthesize the samples without the TX 100 surfactant.

Structure of the samples was investigated using a X- Ray diffractometer Rigaku Ultima IV with CuK_α radiations with help of PDF2 database from International Center for Diffraction Data (ICDD). Chemical properties of samples were measured by a SHIMADZU IRAffinity-1S Fourier Transform Infra Red spectrometer. The optical energy gap of the samples was determined by a Shimadzu 1800 UV/Visible spectrometer. The operating wavelength of the UV/Visible spectrometer was varied from 190 to 1100 nm. Photocurrent and photovoltage were measured in an electrolyte of KI (0.01M) under the illumination of a 100 W filament bulb placed at 4.5 cm from the sample. A platinum electrode and Ag/AgCl electrode were used as counter electrode and reference electrode, respectively. The gap between the sample and counter electrode was 2.5 cm. The distance between the reference electrode and the counter electrode was 1 cm. The separation between the reference electrode and the sample was 1.5 cm. Impedance was measured using a Metrohm Autolab (PGSTAT 128N). Samples deposited on normal amorphous glass substrates were used for XRD, FTIR and UV/Visible spectrometry measurements. Samples fabricated on conductive glass substrates were used for electrical measurements.

3. Results and Discussion:

All the samples described in this section were deposited at spin speed of 2000 rpm for 30 s, and subsequently annealed at 500 ^{0}C for an hour in air. Figure 1 shows the XRD pattern of the CuO film prepared with the TX 100 surfactant. The XRD patterns of the CuO films without the TX 100 surfactant were presented in some of our previous manuscripts [4, 12]. XRD patterns of the CuO films with and without the TX 100 surfactant were exactly the same by implying that the addition of the TX 100 surfactant does not alter the structure of the CuO film. However, the intensities of peaks of the XRD pattern with the TX 100 surfactant were higher than those of the XRD pattern without the TX100

ISSN 1512-1461

surfactant. Crystallite size (D) and strain (ε) were estimated using $D = \frac{0.91\lambda}{\beta \cos\theta}$ and $\varepsilon = \frac{\beta \cos\theta}{4}$, respectively, where λ is the wavelength of Cu-K_α radiation (λ=1.54060 ^{0}A), and β is the full width of half maxima (FWHM) for XRD peak at angle θ. The crystallite size and the strain were found to be 31.13 nm and 0.00113, respectively. The dislocation density found from $\delta = \frac{1}{D^2}$ was 1.041x10^{15} lines/m^2. All these parameters were calculated for (112) peak of XRD pattern. The average values of the crystallite size, the strain and the dislocation density of the CuO thin films synthesized without the TX 100 surfactant were 27 nm, 0.0013 and 1.35x10^{15} lines/m^2, respectively [9]. The crystallite size increased after adding the TX 100 surfactant. The dislocation density and strain decreased after adding the TX 100 surfactant.

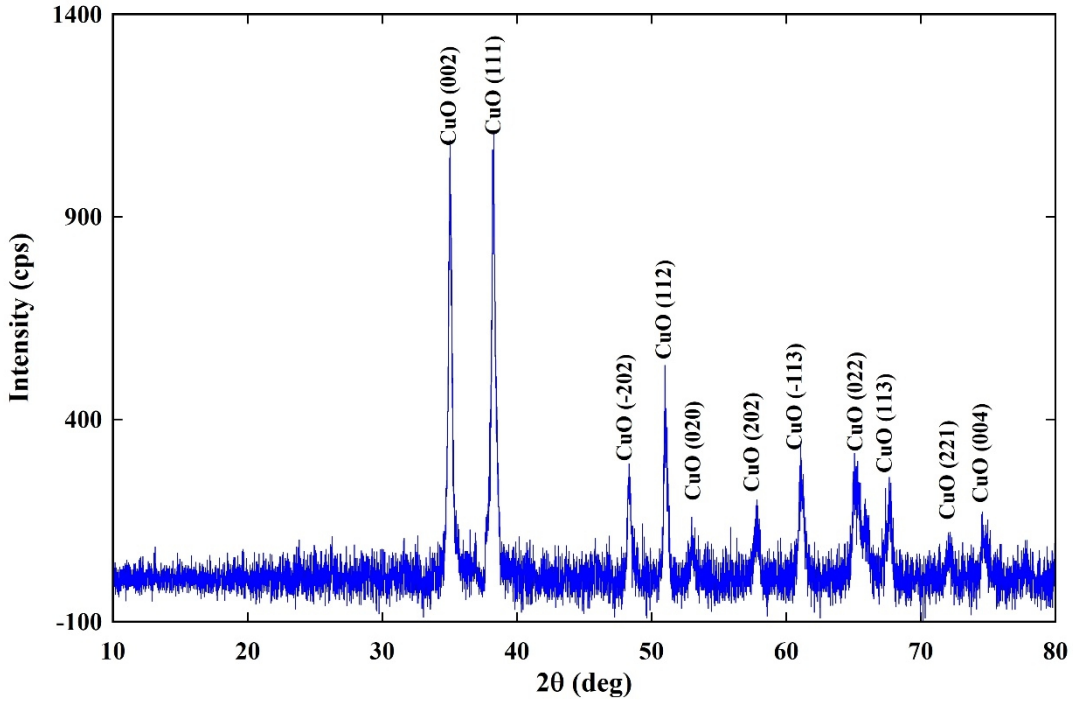

Figure 1: XRD pattern of the CuO film with the TX 100 surfactant.

Figure 2 indicates the FTIR spectrum of the CuO film prepared with the TX 100 surfactant. FTIR peaks can be observed at 537, 1592.37 and 3183.89 cm^{-1} by confirming the formation of pure CuO phase [36]. Addition of the TX 100 surfactant has not made any influence on the FTIR spectrum.

ISSN 1512-1461

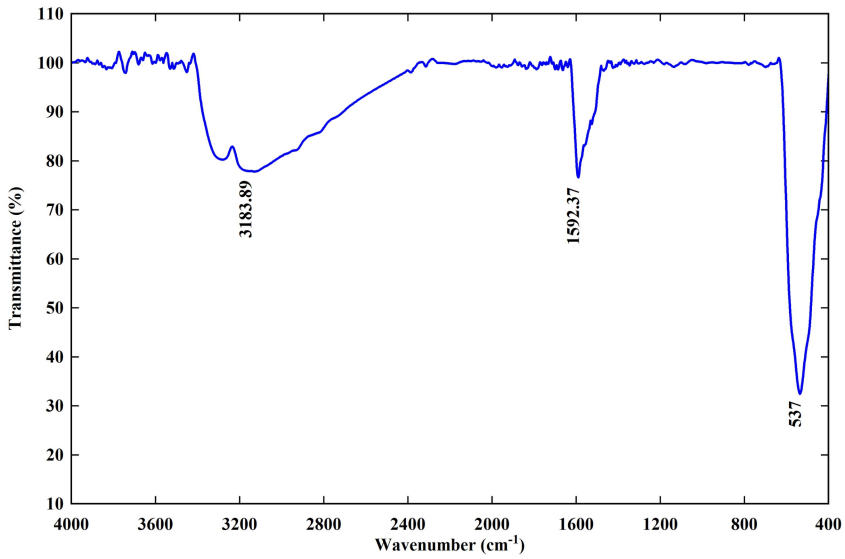

Figure 2: FTIR spectrum of the CuO film prepared with the TX 100 surfactant.

Figure 3 shows the UV visible absorbance spectrums of the CuO film prepared with the TX 100 surfactant. Absorption edge can be observed at 857.25 nm. The optical band gap corresponding to this absorption edge is 1.45 eV. The optical band gap of the CuO films prepared without the TX 100 surfactant was 1.43 eV [12]. The optical band gap of CuO film prepared with the TX 100 surfactant is higher compared to the optical band gap of the CuO films synthesized without the TX 100 surfactant [12].

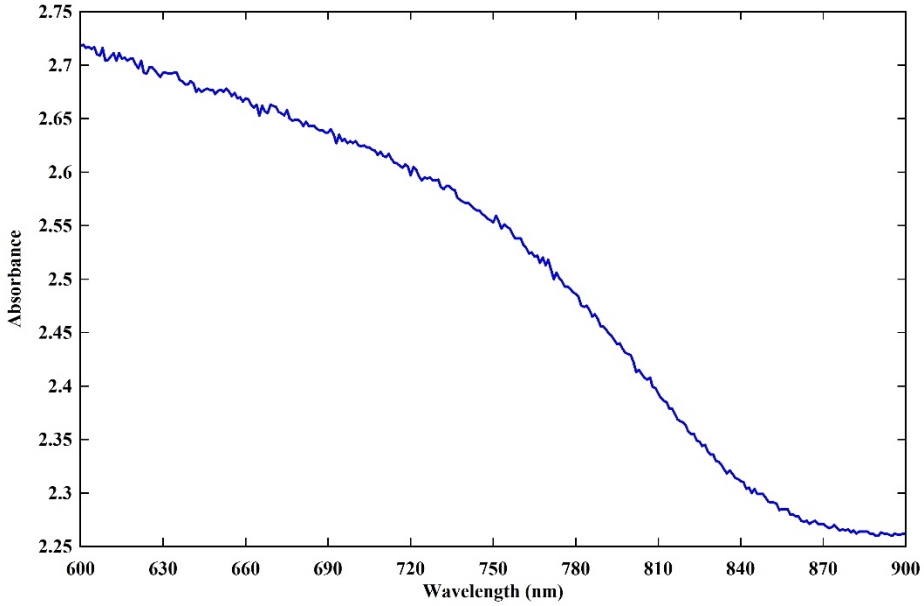

Figure 3: UV visible absorbance spectrums of the CuO film prepared with the TX 100 surfactant.

ISSN 1512-1461

Figure 4 represents the I-V curves of the CuO film with the TX 100 surfactant. Solid and dark curves indicate I-V curves under light and dark conditions. Light and dark currents are -14.25 and 8.05 μA/cm^2, respectively. Light and dark voltages are 0.0594 and -0.1787 V, respectively. Figure 5 shows the graph of photocurrent versus photovoltage of the same sample. Photocurrent, photovoltage and output power of the CuO sample with the TX 100 surfactant are -23.66 μA/cm^2, 0.20 V and 4.732 μW/cm^2, respectively. The maximum photocurrent , the maximum photovoltage and the maximum output power of the CuO sample without the TX 100 surfactant were 11.15 μA/cm^2, 0.117 V and 1.11 μW/cm^2, respectively [4]. Due to the addition of the TX 100 surfactant, the photocurrent, photovoltage and the output power enhanced by factors of 2.12, 1.71 and 4.26, respectively. Electrical properties of materials can be improved by adding the TX 100 surfactant as described below.

TX 100 is a nonionic surfactant with a higher viscosity consisting of hydrophilic polyethylene oxide chains. The surface tension of aqueous solutions can be reduced by adding the TX 100 surfactant. TX 100 is also used as a micellar catalyst in biology. The photocurrent of the samples enhances due to the increase of the mobility of ions after adding the TX 100 surfactant [37]. Peak current of riboflavin has been improved by adding anionic surfactants [38]. Oxidation of acetaminophen (ACOP), aspirin (ASA) and caffeine (CF) can be facilitated at an in-situ TX 100 surfactant modified multiwalled carbon nanotube paste electrode. After adding the TX 100 surfactant, the peak current of all three molecules enhanced due to the strong adsorption of the TX 100 at the surface of the carbon paste via hydrophobic interactions. TX 100 creates a thin layer on the electrode surface where the molecules are preconcentrated. As a result, more electrons transfer between electrode and molecules [39]. TX 100 has been applied to improve the electrocatalytic activity of screen printed carbon paste electrodes [40].

In addition, the crystallite size has been increased after adding TX 100 surfactant according to our XRD data. The photocurrent and the photovoltage increase with the particles size due to the grain boundary effect [41, 42, 43]. Therefore, the increase of the crystallite size also can be attributed to the improvement of the photocurrent and the photovoltage.

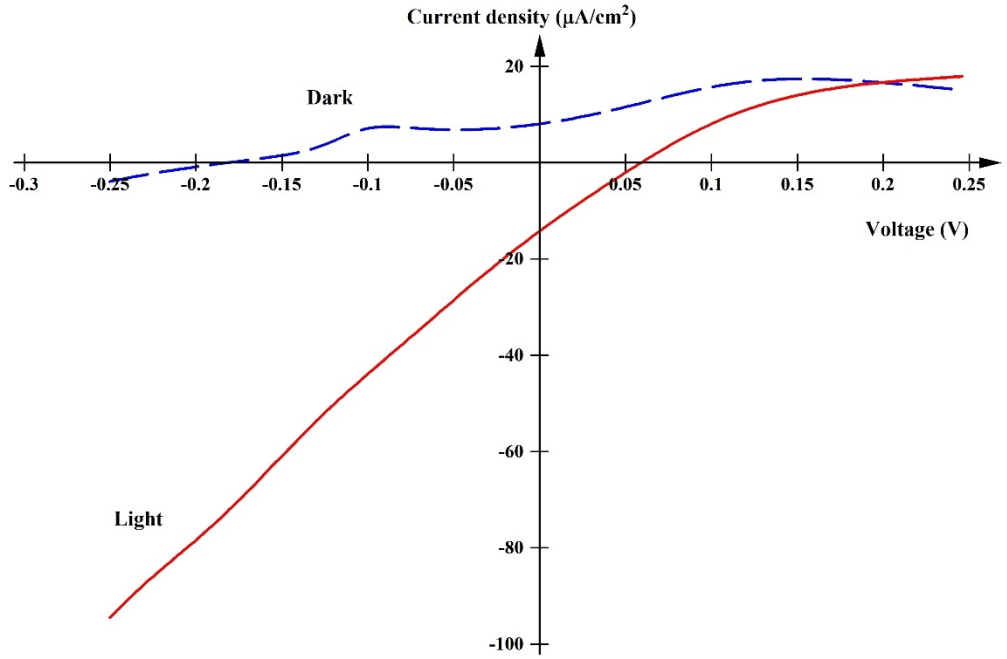

ISSN 1512-1461

Figure 4: I-V curves of the CuO film with the TX 100 surfactant.

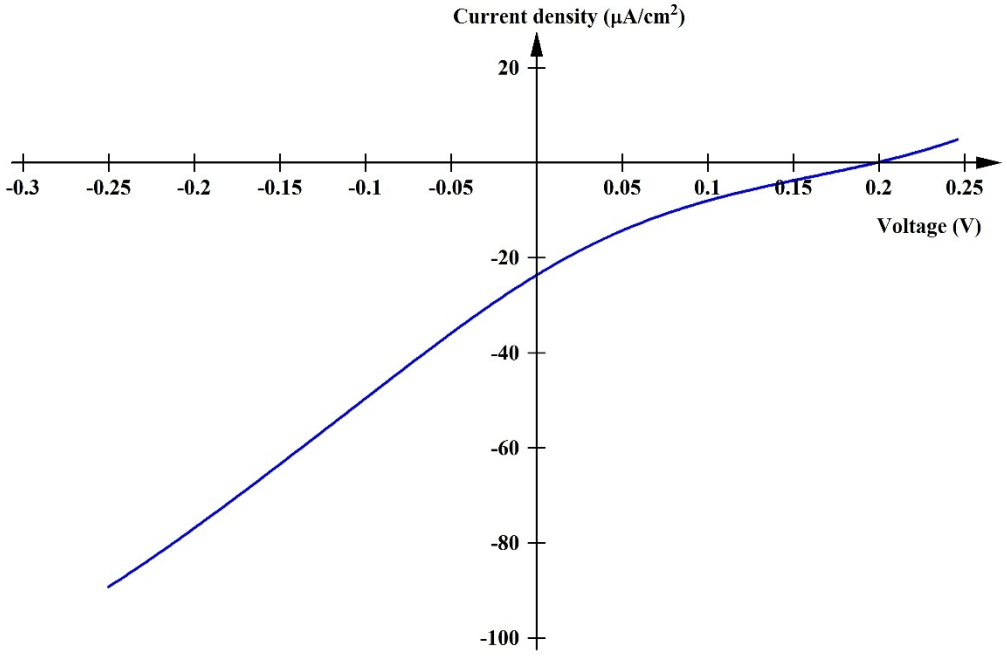

Figure 5: Photocurrent versus photovoltage of the CuO film with the TX 100 surfactant.

Figure 6 shows the impedance curves of the CuO sample with the TX 100 surfactant with and without illumination. Light curve was measured under the illumination of a 100 W filament bulb placed at 4.5 cm from the sample. The imaginary part of dark curve gradually increases with the resistance by indicating the Ohmic behavior. The imaginary part of light curve first increases and then decreases back to its original value by indicating the electrochemical cell behavior. The imaginary part of impedance of dark curve is always higher than that of light curve. Due to the increase of photoconductivity under illumination, the impedance of light curve is always lower than that of dark curve. The impedance curves of the CuO film without the TX 100 surfactant were presented in one of our previous publications [4]. The impedance curves with and without the TX 100 surfactant have some resemblance.

ISSN 1512-1461

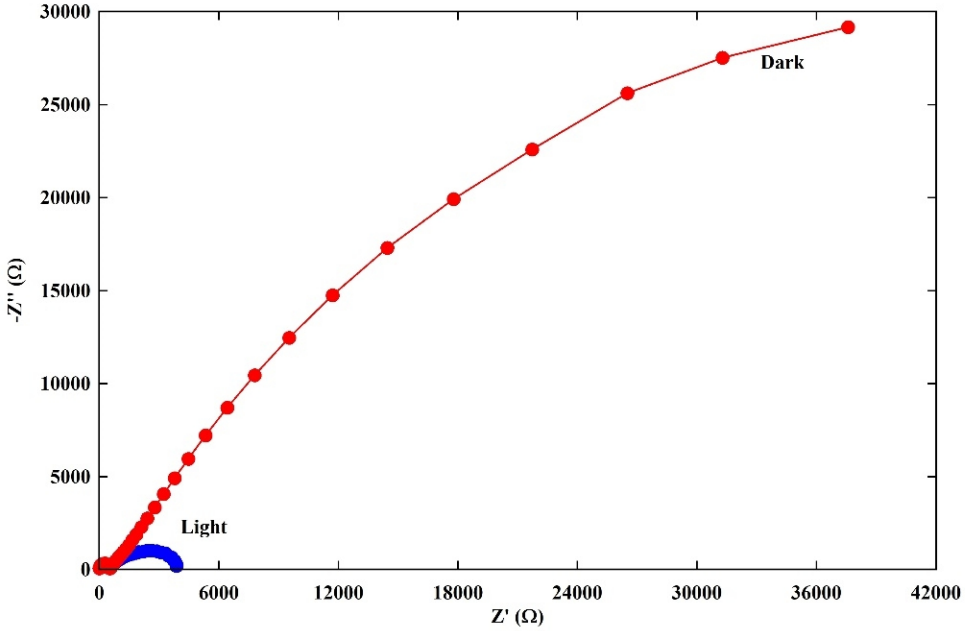

Figure 6: Impedance curves of the CuO sample with the TX 100 surfactant.

Figure 7 represents the Nyquist plot of initial part of the light curve shown in figure 6. Each semicircle related to a RC parallel circuit. Two semicircles represent the charge transfer at the Pt/electrolyte and sample/electrolyte interface in the cell [44]. Resistance values estimated for the charge transfer at Pt/electrolyte and sample/electrolyte were found to be 500 and 3350 Ω, respectively. Three semicircles were observed for the samples fabricated without the TX 100 surfactant corresponding to Pt/electrolyte, sample/electrolyte and electrolyte diffusion impedance [4]. However, the semicircle corresponding to the electrolyte diffusion impedance is vanished in the plot of the CuO sample with the TX 100 surfactant. This is attributed to the enhancement of electrical properties of the sample due to the TX 100 surfactant. According to the Nyquist plots of CuO films with and without the TX 100 surfactant, the resistance value related to the charge transfer at Pt/electrolyte does not change due to the addition of the TX 100 surfactant [4].

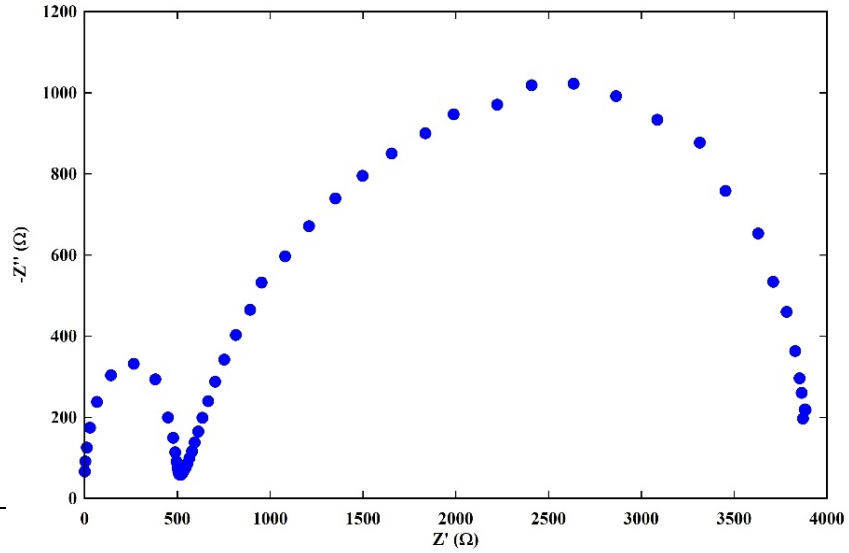

Figure 7: Nyquist plot of initial part of the light curve.

ISSN 1512-1461

Figure 8 shows the Bode plot of the CuO sample with the TX 100 surfactant. Red and blue curves indicate dark and light curves, respectively. At higher frequencies, both light and dark curves overlap. However, at lower frequencies dark curve shows higher impedance values compared to the light curve. Because the concentration of conduction electrons increases after illuminating the sample, the impedance decreases due to the illumination. At very high frequencies, rapid decrease of impedance of dark curve can be observed.

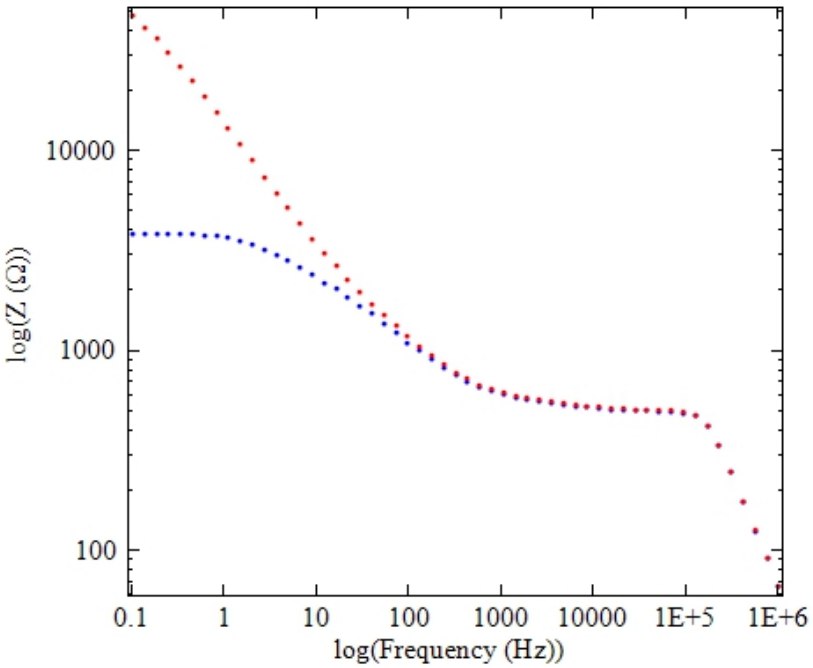

Figure 8: Bode plot the CuO sample with the TX 100 surfactant.

Figure 9 represents the Bode phase plots of the CuO sample with the TX 100 surfactant. Here red and blue curves show dark and light curves, respectively. Peaks can be observed at mid and high frequency regions. The electron lifetime (τ_e) has been estimated for the peak at mid frequency region using $\tau_e = \frac{1}{2\pi f_{mid}}$ [45]. The mid peak frequencies for light and dark curves are 59.41 and 1.63 Hz, respectively. The estimated values of electron lifetimes for light and dark curves are 2.68 and 97.81 ms, respectively. Under the illumination, the mobility of the charge carriers is higher. As a result, charges can easily recombine. Therefore, the electron lifetime of the sample under illumination is less than that of the each sample without illumination.

ISSN 1512-1461

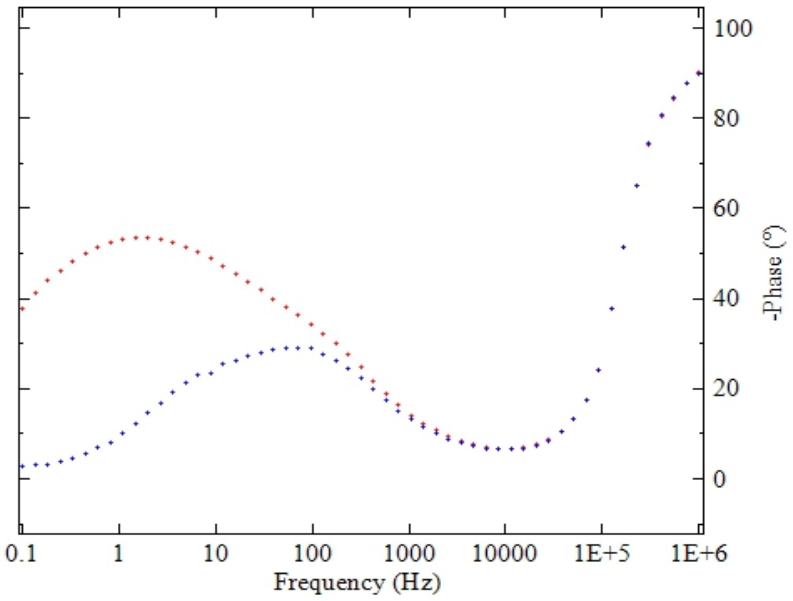

Figure 9: Bode phase plots of the CuO sample with the TX 100 surfactant.

Figure 10 shows the Bode phase plot of a CuO thin film synthesized without the TX 100 surfactant. The red and blue curves show dark and light curves, respectively. Above the frequency of 10 HZ, the dark and light curves overlap. The peaks of light and dark curves can be observed at 2.61 and 0.68 Hz, respectively. The electron life times calculated from $\tau_e = \frac{1}{2\pi f_{mid}}$ were found to be 61 and 233 ms with and without illumination, respectively. Electron life times decrease after adding the TX 100 surfactant. Because the TX 100 surfactant behaves as a catalyst, the mobility of the electrons is higher in the sample with the TX 100 surfactant. The collision and the recombination rates are higher when the mobility is higher. Therefore, the electron life time reduce due to the higher mobility.

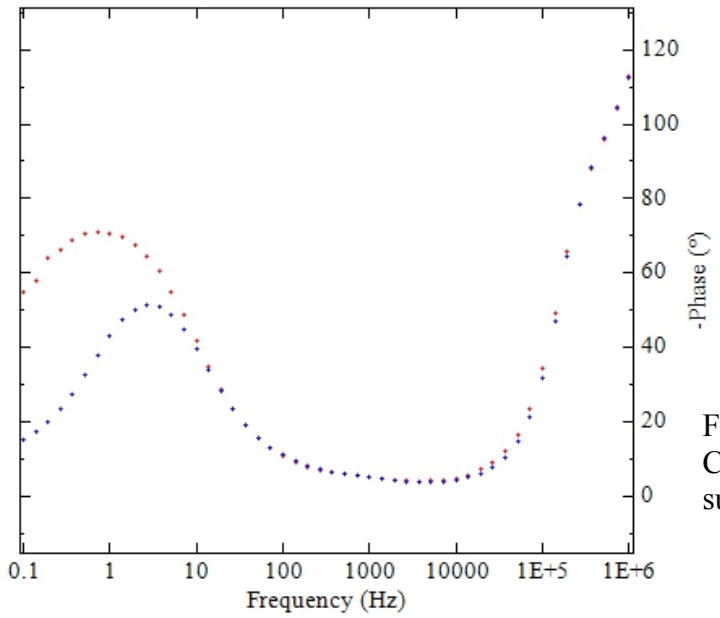

Figure 10: Bode phase plot of a CuO thin film without the TX 100 surfactant.

ISSN 1512-1461

4. Conclusion:

The photocurrent, photovoltage and the output power of the liquid junction photocell prepared with the CuO thin films and KI electrolyte can be enhanced by adding the TX 100 surfactant. TX 100 surfactant serves as a catalyst in the sample and enhances the photovoltaic properties. In addition, the strong adsorption via hydrophobic interactions and electrocatalytic activity of the TX 100 surfactant enhance electrical properties of the liquid junction photocell. The crystallite size of the CuO thin film increases after adding the TX 100 surfactant. As a result, the photocurrent and photovoltage enhance due to the grain boundary effect. The photocurrent, photovoltage and output power of the CuO sample with the TX 100 surfactant are -23.66 $\mu A/cm^2$, 0.20 V and 4.732 $\mu W/cm^2$, respectively. The optical band gap slightly increases from 1.43 to 1.45 eV after adding the TX 100 surfactant. FTIR peaks can be observed at 537, 1592.37 and 3183.89 cm^{-1} by indicating the synthesis of CuO in thin film form. According to the Nyquist plots, resistance values estimated for the charge transfer at Pt/electrolyte and sample/electrolyte interfaces were 500 and 3350 Ω, respectively. According to the Bode phase diagrams, the electron lifetimes of the CuO samples with the TX 100 surfactant under light and dark conditions are 2.68 and 97.81 ms, respectively. The electron lifetimes of the CuO samples without the TX 100 surfactant under light and dark conditions are 61 and 233 ms, respectively.

References:

1. X. Zeng, J. Ma, J. Su, L. Zhou, J. Zhang and L. Li, Materials Research Express (2017), 4(4), article ID 045009.
2. X**.** Li, X. Xiong and Q. Zhang, Materials Research Express (2017), 4(4), article ID 045018.
3. A. Szkudlarek, K. Kollbek, S. Klejna and A. Rydosz, Materials Research Express (2018), 5(12), article ID 126406.
4. P. Samarasekara, P.G.D.C.K. Karunarathna, H.P. Weeramuni and C.A.N. Fernando, Materials Research Express (2018), 5(6), article ID 066418.
5. O. Gencyilmaz and T. Taskopru, Journal of Alloys and Compounds (2016), 695, 1205.
6. M. Dahrul, Alatas Husin, Irzaman, Procedia Environmental Sciences (2016), 33, 661
7. S. Dolai, R. Dey, S. Das, S. Hussain, R. Bhar and A.K. Pal, Journal of Alloys and Compounds (2017), 724, 456.
8. Dhaouadi Mehdi, Jlassi Mohamed, Sta Imen, Miled Islem Ben, Mousdis George, Kompitsas Micheal and Dimassi Wissem, American Journal of Physics and Applications (2018), 6(2), 43.
9. P. Samarasekara, P.G.D.C.K. Karunarathna, B.M.C.M. Bandaranayake, J.S.T. Wickramasinghe and C.A.N. Fernando, Materials Research Express (2018), 6(3), article ID 036415.
10. A.S. Bhattacharyya, S.K. Raj, Parameshwar Kommu, P. Prabhakar, R. Praveen Kumar, Neha Kumari and Kumar Gaurav, Surface and Interface Analysis (2016). 48, 1294.
11. K.S. Wanjala, W.K. Njoroge, N.E. Makori and J.M. Ngaruiya, American Journal of Condensed Matter Physics (2016), 6(1), 1.
12. P. Samarasekara, P.G.D.C.K. Karunarathna, H.P. Weeramuni and C.A.N. Fernando, Georgian Electronic Scientific Journals: Physics (2018), 1(18), 13.
13. H.Z. Asl and S.M. Rozati, Materials Research (2018), 21 (2), article ID e20170754.
14. O. Daoudi, Y. Qachaou, A. Raidou, K. Nouneh, M. Lharch and M. Fahoume, Superlattices and Microstructures (2018), 127, 93.
15. K. Iqbal, M. Ikram, M. Afzal and S. Ali, Materials for Renewable and Sustainable Energy (2018), 7, 4.
16. C.H. Tsai, P.H. Fei, C.M. Lin and S.L. Shiu, Coatings **(**2018), 8(1), 21.

ISSN 1512-1461

17. D.S. Zimbovskii and B.R. Churagulov, Inorganic Materials (2018), 54 (7), 660.
18. T.T. Li, N. Bao, A.F. Geng, H. Yu, Y. Yang and X.T. Dong, Royal Society Open Science (2018), 5(2), 171788.
19. B. Sahin and R. Aydin, Journal of Natural Applied Sciences (2018), 22(2), 545.
20. K. Mikami, Y. Kido, Y. Akaishi, A. Quitain and T. Kida, Sensors (2019), 19(1), 211.
21. D. Predoi, S.L. Iconaru, M.V. Predoi, N. Buton and M.M. Heino, Coatings (2019), 9(3), 156.
22. T.S. Roopa, H.N.N. Murthy, H.S. Swathi, G. Angadi and D.V.N. Harish, Bulletin of Materials Science (2019), 42, 15.
23. N.B. Patil, A.R. Nimbalkar and M.G. Patil, Materials science and Engineering B (2018), 227, 53.
24. H.A. Dehkordi, A. Mokhtari, K. Dastafkan and Soleimanian, Journal of Electronic Materials (2019), 48(2), 1258.
25. S. Belhamri and N. Hamdadaou, Surface Review and Letters (2018), 25(4), article ID 1850092.
26. P. Samarasekara, Chinese Journal of Physics (2009), 47(3), 361.
27. H. Hegde, P. Samarasekara and F.J. Cadieu, Journal of Applied Physics (1994), 75(10), 6640.
28. P. Samarasekara and N.U.S. Yapa, Sri Lankan Journal of Physics (2007), 8, 21.
29. P. Samarasekara and Udara Saparamadu, Georgian electronic scientific journals: Physics (2012), 1(7), 15.
30. P. Samarasekara, Inventi Rapid: Algorithm Journal (2011), 2(1), 1.
31. P. Samarasekara and N.H.P.M. Gunawardhane, Georgian electronic scientific journals: Physics (2011), 2(6), 62.
32. P. Samarasekara and William A. Mendoza, Georgian Electronic Scientific Journals: Physic*s* (2011), 1(5), 15.
33. P. Samarasekara and William A. Mendoza, Electronic Journal of Theoretical Physics (2010), 7(24), 197.
34. P. Samarasekara, Electronic Journal of Theoretical Physics (2007), 4(15), 187.
35. P. Samarasekara, M.K. Abeyratne and S. Dehipawalage, Electronic Journal of Theoretical Physics (2009), 6(20), 345.
36 J. Jayaprakash, N. Srinivasan, P. Chandrasekaran and E.K. Girija, Spectrochimica Acta Part A: Molecular and Biomolecular Spectroscopy (2015), 136(c), 1803.
37. A. Mohammad, E. Iraqi and I.A. Khan, Journal of Chromatographic Science (2002), 40, 162.
38. P.V. Jaiswal, V.S. Ijeri and A.K. Srivastava, Analytical Sciences (2001), 17, i741.
39. B. Sanghavi and A. Srivastava, Electrochimica Acta (2010), 55(28), 8638.
40. C.J. Yuan, Y.C. Wang and O. Reiko, Analytica Chimica Acta (2009), 653, 71.
41 M.K. Sharma and D.P. Joshi, Indian Journal of Pure and Applied Physics (2010), 48, 575.
42. S.S. Chu, T.L. Chu and H.T. Yang, Applied Physics Letters (1978), 32, 557.
43. Y.C.M. Yeh, K.L. Wang, B.K. Shin and R.J. Stirn, Proceedings of the 14th IEEE Photovoltaic Specialists Conference (Kissimmee IEEE, New York) (1980), 1338.
44. R. Kern, R. Sastrawan, J. Ferber, R. Stangl and J. Luther, Electrochimica Acta (2002), 47, 4213.
45. J.H. Park, S.W. Seo, J.H. Kim, C.J. Choi, H. Kim, D.K. Lee, W.S. Jung and K.S. Ahn, Molecular Crystals and Liquid Crystals (2011), 538, 285.

Article received: 2020-08-17